Energy 35 (2010) 3891–3901

Contents lists available at ScienceDirect

Energy

journal homepage: www.elsevier.com/locate/energy

# Performance analysis of a direct expansion air dehumidification system combined with membrane-based total heat recovery

Cai-Hang Liang, Li-Zhi Zhang*, Li-Xia Pei

*Key Laboratory of Enhanced Heat Transfer and Energy Conservation of Education Ministry, School of Chemistry and Chemical Engineering, South China University of Technology, Guangzhou 510640, China*

ARTICLE INFO

*Article history:*
Received 3 November 2009
Received in revised form
31 May 2010
Accepted 3 June 2010

*Keywords:*
Membrane
Total heat recovery
Dehumidification
Direct expansion
Modeling

ABSTRACT

A direct expansion (DX) air dehumidification system is an efficient way to supply fresh and dry air to a built environment. It plays a key role in preventing the spread of respiratory disease like Swine flu (H1N1). To improve the efficiency of a conventional DX system in hot and humid regions, a new system of DX in combination with a membrane-based total heat exchanger is proposed. Air is supplied with dew points. A detailed mathematical modeling is performed. A cell-by-cell simulation technique is used to simulate its performances. A real prototype is built in our laboratory in South China University of Technology to validate the model. The effects of inlet air humidity and temperature, evaporator and condenser sizes on the system performance are investigated. The results indicate that the model can predict the system accurately. Compared to a conventional DX system, the air dehumidification rate (ADR) of the novel system is 0.5 times higher, and the coefficient of performance (COP) is 1 times higher. Furthermore, the system performs well even under harsh hot and humid weather conditions.



## 1. Introduction

Indoor air quality has gained much attention recently [1–4]. Besides violate organic compounds (VOCs), humidity is another key factor influencing thermal comfort and indoor air quality. Fresh air ventilation is an efficient way to control indoor air quality and humidity. It is also helpful for the prevention of respiratory disease like swine flu (H1N1). Outside air humidity stays above 80–90% continuously for a dozen of days in subtropical regions like South China. It is necessary to dehumidify fresh air before it can be supplied to buildings. Air dehumidification has played a crucial role in modern air conditioning industry which tends to separate the treatment of latent load from sensible load [5–7].

The mechanical direct expansion (DX) air dehumidification system is widely used. It has some coherent advantages. It is mature and compact. It can be moved freely in a room. It only uses electricity, which is convenient in urban apartments. In contrast, other technologies like absorption columns and desiccant wheels need outside heat sources to regenerate, which is hard to find in urban areas. Due to these reasons, there have been many studies in DX air dehumidification systems [8–10].

However, a conventional DX system consumes a lot of electric energy. Further, the coefficient of performance (COP) deteriorates fast under hot and humid operating conditions. The energy cost will be huge if the ventilation rates are set high to control indoor air quality. Consequently new dehumidification systems are desired.

Recently, a new DX system in combination with a membrane-based total heat exchanger has been proposed [11–13], as shown in Fig. 1. The fresh air is first dehumidified and cooled by the exhaust air in a total heat exchanger. Cool and dryness are recovered to the fresh air from the exhaust air. Then the fresh air is further cooled and dehumidified to the set points by a DX system. The sensible effectiveness of the total heat exchanger can be as high as 0.75, and the latent effectiveness can be as high as 0.65 [7]. Since most of the sensible and latent loads are treated by the total heat exchanger, a large fraction of the energy is saved.

The technology provides a solution to air dehumidification with high-energy efficiency. Previous efforts were concentrated only on its feasibility studies. The performance of the system is seldom investigated in detail. In the present work, a cell-by-cell modeling approach recently developed by Liang et al. [14] is used to predict the performances of this system. Further, an experimental set-up was built to validate the model and to evaluate performances, which is a continuation of a series of studies on heat and moisture recovery and air dehumidification in South China University of Technology.

In Ref. [14], an auxiliary condenser is used to re-heat the dehumidified air to prevent cold drat, which makes the system

* Corresponding author. Tel./fax: +86 20 87114268.
*E-mail address:* Lzzhang@scut.edu.cn (L.-Z. Zhang).

0360-5442/$ – see front matter © 2010 Elsevier Ltd. All rights reserved.
doi:10.1016/j.energy.2010.06.002

**Nomenclature**

| | |
|---|---|
| $A$ | area ($m^2$) |
| ADR | air dehumidification rate (kg $h^{-1}$) |
| $b_w$ | slope of $H$ vs $T$ curve |
| $c_{p,a}$ | specific heat (kJ $kg^{-1}$ $K^{-1}$) |
| $C_v$ | flow coefficient |
| COP | coefficient of performance |
| $d$ | diameter (m) |
| $h_c$ | airside convective heat transfer coefficient (kW $m^{-2}$ $K^{-1}$) |
| $h_m$ | convective mass transfer coefficient (kg $m^{-2}$ $s^{-1}$) |
| $h_r$ | refrigerant side convective heat transfer coefficient (kW $m^{-2}$ $K^{-1}$) |
| $H$ | specific enthalpy (kJ $kg^{-1}$) |
| $k$ | thermal conductivity (W $m^{-1}$ $K^{-1}$) |
| $\dot{m}$ | mass flow rate (kg $s^{-1}$) |
| $N$ | compressor speed (rpm) |
| NTU | number of transfer units |
| $p$ | pressure (Pa) |
| $P$ | perimeter (m) |
| $Q$ | cooling power (kW) |
| $S$ | slip ratio |
| SHR | sensible heat ratio |
| $T$ | temperature (°C) |
| $u$ | mass flux (kg $s^{-1}$ $m^{-2}$) |
| UA | global heat transfer coefficient (W $K^{-1}$) |
| $v$ | specific volume ($m^3$ $kg^{-1}$) |
| $V$ | volumetric air flow rate ($m^3$ $s^{-1}$) |
| $W$ | electric power (W) |
| $X$ | spatial coordinate (m) |
| $\Delta y$ | absolute error |
| $\Delta y/y$ | relative error (%) |
| $\Delta p$ | pressure drop (Pa) |
| $\Delta T_{sh}$ | superheating (°C) |
| $\Delta T_{sc}$ | subcooling (°C) |
| $\Delta T$ | Temperature difference between supply air and indoor air (°C) |
| $\eta_i$, $\eta_{mo}$ and $\eta_{me}$ | indicated efficiency, motor efficiency and mechanical efficiency |

*Greek letters*

| | |
|---|---|
| $\alpha$ | vapor quality |
| $\beta$ | ratio of latent to sensible total transfer units |
| $\sigma$ | ratio of the dead space to the swept volume (e) |
| $\rho$ | density (kg $m^{-3}$) |
| $\varepsilon$ | effectiveness |
| $\omega$ | humidity ratio (kg moisture/kg air) |
| $\varphi$ | relative humidity |
| $\psi$ | ratio of diffusive to convective moisture resistance for membrane |

*Subscripts*

| | |
|---|---|
| a | air |
| ao | air at the evaporator exit |
| c | condensation |
| cacl | calculated |
| circ | circulated |
| com | compressor |
| d | dead space volume ($m^3$) |
| DX | direct expansion |
| elec | electrical |
| e | evaporator |
| ex | exhaust |
| exp | experiment |
| f | inlet air |
| i | inlet, inside |
| l | liquid |
| L | latent |
| mem | membrane |
| me | mechanical |
| o | outside, outlet |
| r | refrigerant |
| sat | saturation |
| suc | suction |
| sup | supply |
| sw | swept volume ($m^3$) |
| S | sensible |
| tot | total |
| txv | thermal expansion valve |
| v | gas |
| w | wall |
| wat | water |

complicated. This study uses only one condenser, so it is simple. However how does it affect the thermal comfort? This question should be considered, since it supplies air directly with dew points.

## 2. System description and experimental set-up

### 2.1. System description

A schematic diagram of the present system is shown in Fig. 1. As shown, the system is composed of a membrane-based total heat exchanger and a DX air dehumidification system. The total heat exchanger is in parallel-plates structure. The material is a self-developed novel vapor-permeable membrane, which has high vapor permeability [15]. Fresh air (state E) passes through the total heat exchanger, where the incoming fresh air exchanges moisture and temperature simultaneously with the exhaust air. As a result, the total heat (cool and dryness) is recovered from the exhaust air. Fresh air leaving the total heat exchanger (state B) is cool and dry. Then the cool and dry fresh air is further cooled and dehumidified below dew point in the evaporator. Fresh air at this temperature (state C) is directly supplied to the room, which is called dew point ventilation. The incoming fresh air extracts excess heat and moisture from the room before its temperature and humidity reach the indoor air states finally.

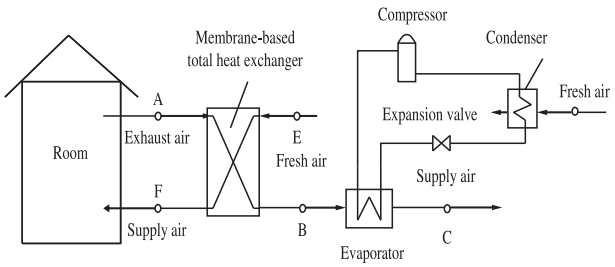


**Fig. 1.** Schematic of a DX air dehumidification system combined with membrane-based total heat recovery.

**Table 1**
Geometrical and physical properties of the main components.

| Parameter | Description or value | Parameter | Description or value |
|---|---|---|---|
| Compressor | | Evaporator | |
| Compressor type | Reciprocating | Coil face width | 240 mm |
| Swept volume | 10.0 $cm^3$ | Coil face height | 15 mm |
| Rating cooling power | 0.945 kW | Coil face depth | 87 mm |
| Rating power consumption | 0.315 kW | Number of tube rows | 4 |
| Membrane-based total heat exchanger | | Number of tubes in each row | 6 |
| Number of channels for each flow | 115 | Tube material | Copper |
| Channel length | 185 mm | Tube arrangement | Staggered |
| Channel width | 185 | Transverse tube spacing | 21.65 mm |
| Channel pitch | 2 mm | Longitudinal tube spacing | 25.4 mm |
| Channel type | Parallel | Tube thickness | 0.035 mm |
| Condenser | | Inside tube diameter | 9.3 mm |
| Coil face width | 400 mm | Outside tube diameter | 10.0 mm |
| Coil face height | 150 mm | Collar diameter | 10.24 mm |
| Coil face depth | 87 mm | Fin type | Corrugated |
| Number of tube rows | 4 | Corrugated height | 0.8 mm |
| Number of tubes in each row | 6 | Fin material | Aluminium |
| Coil total external surface area | 5.26 $m^2$ | Fin thickness | 0.12 mm |
| Thermal expansion valve | | Fin spacing | 1.8 mm |
| Rating cooling power | 1.0 kW | Coil total external surface area | 3.15 $m^2$ |

Notes: The geometrical and physical properties of the condenser are not listed in the table, which is the same as that of evaporator.

The difference between this study and Ref. [14] is that a separate flow model is used to model the two-phase zone in this paper. In contrast, a homogeneous flow model is used to model the two-phase zone in Ref. [14]. Some equations of the two papers are similar since they employ the same equipments. However, systems are different. There are two parallel condensers in Ref. [14]. The supply air temperatures are set to 20 °C by controlling the refrigerant mass flow ratios between the main and the auxiliary condensers. In contrast, there is only one condenser in this system, and the refrigerant is not divided. This different configuration will have great differences in the performances for the two systems. How does the new system perform is the subject of this study.

### 2.2. Experimental set-up

The experimental set-up is shown in Fig. 2. It consists of four sections: a wind tunnel, an air handling system, a DX air dehumidification system, and an instrumentation and data acquisition system. The wind tunnel is an open circuit, delivery-type rectangular duct. Air is forced through the tunnel using a variable speed centrifugal blower. The blower is connected to the diverging section of the tunnel through a flexible coupling to avoid noise and vibration. The tunnel walls are thermally insulated by 30 mm thick rubber plastic insulation materials. The air handling system provides the required air states. It consists of a variable output steam humidifier

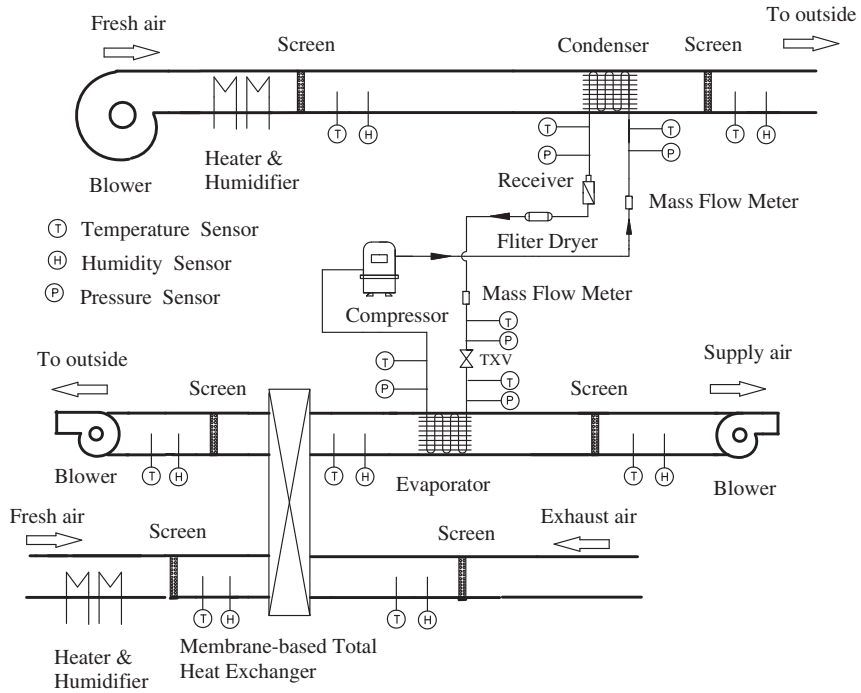


**Fig. 2.** Experimental rig of a DX air dehumidification system combined with membrane-based total heat recovery.

and a variable output electric heater. The novel DX air dehumidification system consists of a membrane-based total heat exchanger, a reciprocating compressor, a condenser, a receiver, a filter, a dryer, a thermal expansion valve (TVX), and an evaporator. R22 is used in the present refrigeration system because it is easily available from local retail stores. The physical design parameters of the main components of the system are listed in Table 1. The whole system is constructed in an air-conditioned room, so inlet air states can be preset first. The nominal air-conditioned states for exhaust air (indoor environment) are 27 °C and 53% RH. The data acquisition and instrumentation system of the test rig has been described in [14].

### 2.3. Uncertainty analysis

Uncertainty analysis for the experimental results is estimated using expressions by Guttmann et al. [16].

$$\Delta y = \left[\left(\frac{\partial f}{\partial x_1}\right)^2(\Delta x_1)^2+\left(\frac{\partial f}{\partial x_2}\right)^2(\Delta x_2)^2+\cdots+\left(\frac{\partial f}{\partial x_n}\right)^2(\Delta x_n)^2\right]^{\frac{1}{2}} \tag{1}$$

$$\frac{\Delta y}{y} = \left[\left(\frac{\partial f}{\partial x_1}\right)^2\left(\frac{\Delta x_1}{y}\right)^2+\left(\frac{\partial f}{\partial x_2}\right)^2\left(\frac{\Delta x_2}{y}\right)^2+\cdots + \left(\frac{\partial f}{\partial x_n}\right)^2\left(\frac{\Delta x_n}{y}\right)^2\right]^{\frac{1}{2}} \tag{2}$$

where $f$ is the function of the independent variables. Variables $x_1$, $x_2$, etc., stand for the variables of the functions, $\Delta x_1$, $\Delta x_2$, etc. are the absolute error associated with the variables and $\frac{\Delta y}{y}$ means the relative error.

Based on these relations, a detailed error analysis indicated that an overall uncertainty is within ±6.5% for air dehumidification rate (ADR). An overall uncertainty is within ±7.3% for cooling power (Q). It is within ±8.2% for the thermal COP.

## 3. Mathematical modeling

### 3.1. Membrane-based total heat exchanger

The effectiveness-Number of Transfer Units ($\epsilon$-NTU) method is used in the present investigation. Comparing to finite difference method, the $\epsilon$-NTU method is simple. However, it is fairly accurate to predict the performance of the membrane-based total heat exchanger except extremes of the variables [11,12].

According to the technique, the sensible effectiveness ($\epsilon_S$) is a function of two dimensionless parameter, NTU and $C^0_{min}/C^0_{max}$. $\varepsilon_S$ is calculated by

$$\varepsilon_s = 1-\exp\left[\frac{\exp\left(-\mathrm{NTU}^{0.78}C^0_{min}/C^0_{max}\right)-1}{\mathrm{NTU}^{-0.22}C^0_{min}/C^0_{max}}\right] \tag{3}$$

where NTU is the number heat transfer units, and $C^0_{min}/C^0_{max}$ is the ratio of minimum and maximum heat capacity of the two air streams. NTU is expressed as

$$\mathrm{NTU} = \frac{UA_{tot}}{(\dot{m}_a c_{pa})} \tag{4}$$

where $U$ is the total heat transfer coefficient (kW m$^{-2}$ K$^{-1}$), $A_{tot}$ is the total exchange area (m$^2$), $\dot{m}_a$ is the mass flow rate (kg s$^{-1}$) and $c_{pa}$ is the specific heat of air (kJ kg$^{-1}$ K$^{-1}$).

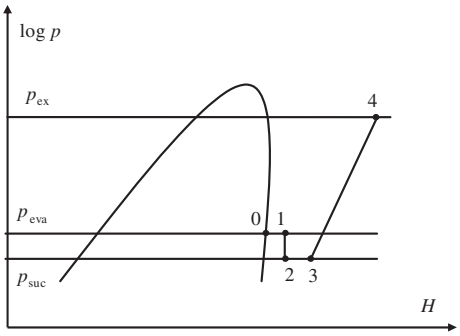


**Fig. 3.** Diagram (log $p$, $H$) of the compression cycle.

The latent effectiveness ($\varepsilon_L$) can be written as:

$$\varepsilon_L = 1-\exp\left[\frac{\exp\left(-\mathrm{NTU}_L^{0.78}\dot{m}_{min}/\dot{m}_{max}\right)-1}{\mathrm{NTU}_L^{-0.22}\dot{m}_{min}/\dot{m}_{max}}\right] \tag{5}$$

$$\mathrm{NTU}_L = \beta\cdot\mathrm{NTU} \tag{6}$$

where $\dot{m}_{min}/\dot{m}_{max}$ is the ratio of minimum air mass flow rate to maximum air mass flow rate. $\beta$ is the ratio of moisture to sensible total transfer units, which is related to material properties. Assuming equal specific heats for two air streams, then $\beta$ can be expressed as:

$$\beta = \frac{1}{1+\psi} \tag{7}$$

where $\psi$ is the ratio of diffusive to convective moisture resistance for membrane.

### 3.2. Compressor

In this study, a simple and thermodynamically realistic model proposed by Duprez [17] is used to evaluate the compressor performance. The mass flow rate, power consumptions and exhaust temperature of compressor are calculated using the model. The input data are the evaporator temperature, condensate temperature and the geometrical parameters. The geometrical parameters are obtained from the manufacturer. The thermodynamic state of the refrigerant through the compressor is presented in Fig. 3.

The thermodynamic parameters of the refrigerant can be calculated, using the Refprop data [18].

The refrigerant mass flow rate is calculated by

$$\dot{m}_{com} = \frac{1}{\nu_3}V_{circ}\frac{N}{60} \tag{8}$$

where $N$ is the compressor speed; $\nu_3$ is the specific volume of refrigerant at point 3. $V_{circ}$, the circulated volume, is the difference volumes between $V_2$ and $V_{3''}$ defined in Crank diagram Fig. 4.

$V_2$ is given by:

$$V_2 = V_d + V_{sw} = \sigma V_{sw} + V_{sw} \tag{9}$$

$V_{3''}$ is calculated by

$$V_{3''} = \nu_{3''}m_{3''} \tag{10}$$

where $\nu_{3''}$ is the specific volume at point 3″, and $m_{3''}$ is gas mass. The expansion process 3′ – 3″ is considered as the isentropic process. The specific volume $\nu_{3''}$ can be calculated from the known pressure and the specific entropy at point 3″.

$m_{3''}$ is calculated by

$$m_{3''} = \frac{V_d}{\nu_{3'}} \tag{11}$$

and

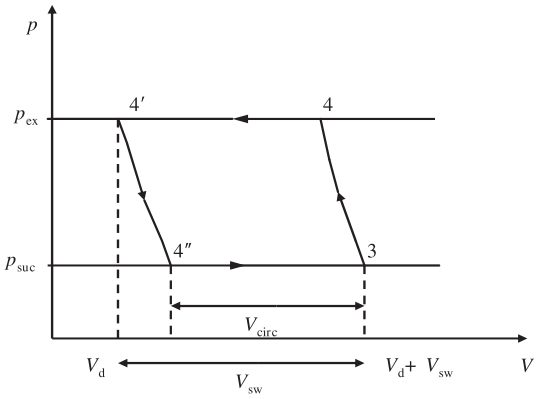


**Fig. 4.** Crank diagram.

$$v_{3'} = v_3 \tag{12}$$

Compressor power is then written by

$$W_{me} = \dot{m}_{com}(H_4 - H_3) \tag{13}$$

The total electrical power work input of the compressor is given by

$$W_{elec} = \frac{W_{me}}{\eta_i \eta_{mo} \eta_{me}} \tag{14}$$

where $\eta_i$, $\eta_{mo}$, and $\eta_{me}$ are the indicated efficiency, motor efficiency and mechanical efficiency, respectively. The values of 0.8, 0.85 and 0.95 are respectively used for them.

### 3.3. Evaporator and condenser

Fin and tube evaporator is used extensively in refrigeration systems. When the temperature of the fin is below the dew points of incoming air, moisture condenses on the surface of the fin, and mass transfer occurs simultaneously with heat transfer. Many different models are found in literature for modeling the evaporator, such as one-zone global models [19], two zone global models [20], tube-by-tube models [21] and cell-by-cell models [22]. Air properties and heat transfer coefficient are assumed to be constant throughout the evaporator in the one zone global models. The evaporator is divided into one single-phase zone and one two-phase zone in two zone global models. The extent of each zone depends on the state of the refrigerant through the evaporator. Each zone has constant air properties. It assumes mean heat transfer coefficients at refrigerant side throughout the zone. Tube-

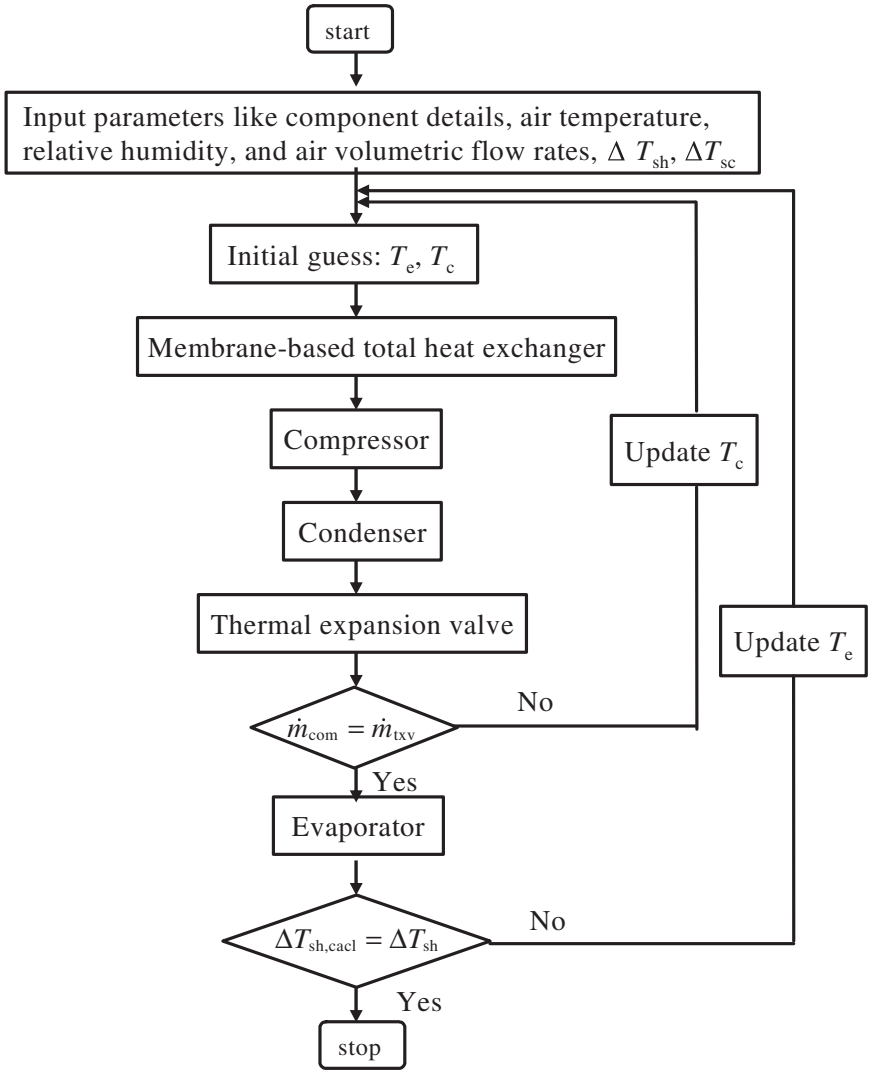


**Fig. 5.** Flow chart for solution procedures of the model.

**Table 2**
The fundamental parameter of the solution procedure.

| Item | Parameters |
|---|---|
| Input data | The geometrical parameters of the component; The fresh air flow rates, The air flow rates through the condenser; The fresh air temperature and humidity; The superheat degree and subcool degree. |
| Initial guess | Evaporator and condenser temperature |
| Convergence criteria | $10^{-6}$ |
| Outputs | The air dehumidification rates; The cooling power; The compressor power consumption; The total power consumption. |

by-tube models take into account the coil circuitry and divide the whole evaporator into tubes, where local properties are used.

However, for air dehumidification, heat transfer and mass transfer occur simultaneously. Air properties are variables throughout the evaporator. In addition, the refrigerant properties like the heat transfer coefficient, frictions factor in the evaporator are variables along a fluid path. These methods are not accurate enough to evaluate the heat and mass transfer performance of the evaporator. Cell-by-cell models are more appropriate. Cell-by-cell models provide the most complete information and best insight into the behavior of the evaporator [23]. According to the technique, the whole evaporator is divided into a number of cells. The governing equations are constructed for each cell. The models also use local air properties and heat transfer coefficient in the energy equation. To simplify the equations, the following assumptions are made:

(1) The refrigerant flow rate is uniform in each circuit, and heat conduction between each circuit is ignored. Therefore, the evaporator may be simplified as one circuit;
(2) The two-phase evaporating flow inside the tube is simplified as a one-dimensional steady and separated flow. The refrigerant liquid and vapor are incompressible and in thermal equilibrium
(3) The axial heat conduction within pipe wall is ignored, as transverse conduction along the fins will be dominant;
(4) The kinetic energy contribution is ignored;
(5) The thermal resistance of metallic element in the system is negligible in comparison with other thermal resistances;
(6) The water condensation outside the tube drops away, with no ice formation occurring.

Based on the above assumptions, the governing equations for refrigerant, tube wall and air can be readily written in the following forms.

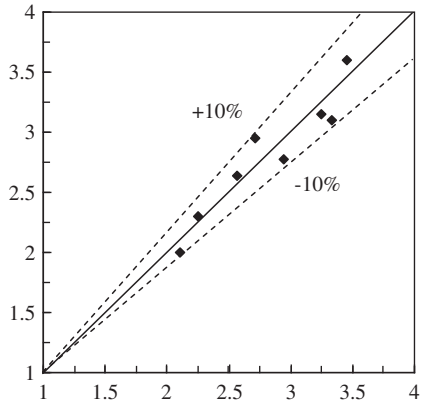


**Fig. 6.** Comparison between experimental air dehumidification rates and calculated air dehumidification rates.

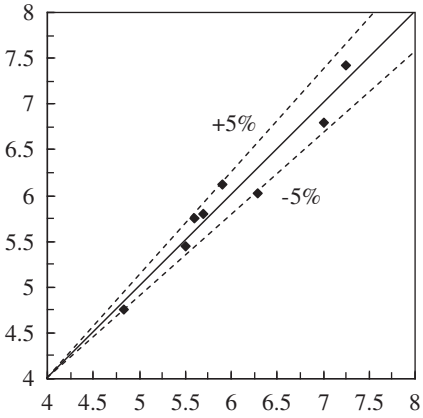


**Fig. 7.** Comparison between experimental COP and calculated COP.

For refrigerant side, the continuity equation can be written as

$$\frac{\partial(\overline{\rho}u)}{\partial X} = 0 \tag{15}$$

where $\overline{\rho}$ is the refrigerant density. For two-phase region, it can be calculated by

$$\overline{\rho} = (1-\alpha)\rho_{\mathrm{l}} + \alpha\rho_{\mathrm{v}} \tag{16}$$

$$\alpha = \frac{1}{1 + S\left(\dfrac{\rho_{\mathrm{v}}}{\rho_1}\dfrac{1-x}{x}\right)} \tag{17}$$

where $\alpha$ is refrigerant void fraction; $x$ is vapour quality; $\rho_{\mathrm{v}}$ and $\rho_{\mathrm{l}}$ are refrigerant vapour density and liquid density, respectively.

$S$ is the slip ratio. A number of correlations can be found in the open literature, for instance in Wallis [24]. The commonly used Chisholm correlation [25] is utilized in this model. The correlation is quite simple and it provides accurate results [26].

$$S = \left[1 - x\left(1 - \frac{\rho_{\mathrm{r,l}}}{\rho_{\mathrm{r,v}}}\right)\right]^{1/2} \tag{18}$$

The energy equation can be written as

$$\frac{\partial(\rho u\overline{H})}{\partial X} = h_{\mathrm{r}}P_{\mathrm{w}}(T_{\mathrm{w}} - T_{\mathrm{r}}) \tag{19}$$

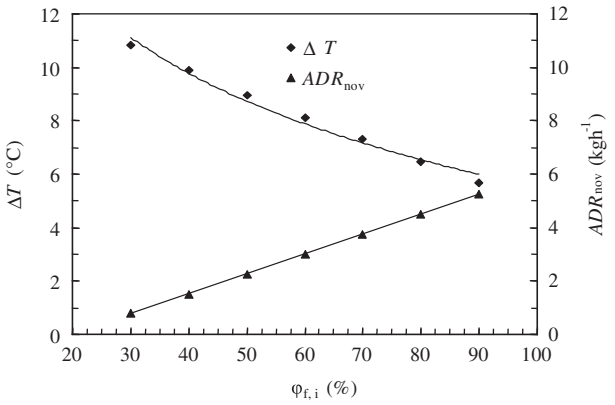


**Fig. 8.** Variations of air dehumidification rates and temperature difference between supply air and indoor air with different inlet air relative humidity.

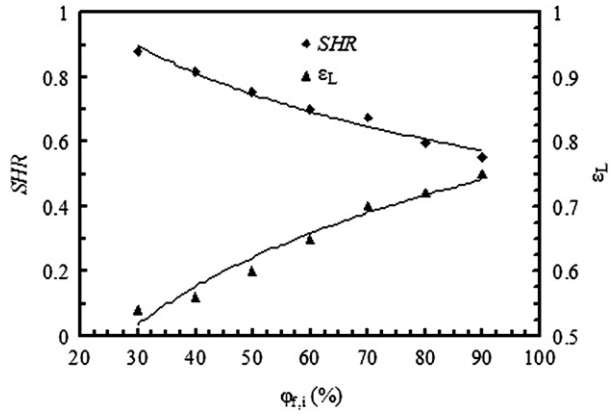


**Fig. 9.** Variations of $\varepsilon_L$ and SHR with different inlet air relative humidity.

where $\overline{H}$is the refrigerant specific enthalpy. In two-phase region, it can be expressed as

$$\overline{H} = (1-\alpha)\rho_l H_l + \alpha\rho_v H_v \tag{20}$$

The pipe wall energy equation can be written as:

$$h_r \pi d_i (T_r - T_w) + h_c A_o (T_{a,i} - T_r) = 0 \tag{21}$$

where $h_r$ is refrigerant side convective heat transfer coefficients. In the single-phase region, the convective heat transfer coefficient is calculated using Ditus–Bollter equation. In the two-phase region, the Kilmenko correlation for heat transfer coefficient is adopted [27].

In airside, air dehumidification takes place on cold surfaces. The conservation equations of energy and mass (moisture) for the cell may be written as:

$$-\dot{m}_a dH_a = dQ - \dot{m}_a d\omega H_{lsat,wat} \tag{22}$$

$$dQ = [h_c(T_a - T_{wat})] + h_m(\omega_a - \omega_{sat,wat}) \times (H_{vsat,t} - H_{lsat,wat})]Pdx \tag{23}$$

$$-\dot{m}_a d\omega = h_m P dx(\omega_a - \omega_{sat,wat}) \tag{24}$$

The dehumidification process is treated using the model by Threleld [28]. The heat transfer can be expressed as a function of enthalpy difference.

$$dQ = \frac{h_{wat}(H_a - H_{s,w})}{b_w} P dx \tag{25}$$

where

$$h_{wat} = \frac{1}{\frac{c_{p,a}}{b_{wat}h_c} + \frac{y_{wat}}{k_{wat}}} P dx \tag{26}$$

in which $k_{wat}$ is the water thermal conductivity, and $y_{wat}$ is the thickness of water film. The value of $y_{wat}/k_{wat}$ is negligible in comparison with other parameters [29]; $h_c$ is airside heat transfer coefficient.

Convective mass transfer coefficient, $h_m$ can be estimated from convective heat transfer coefficient by

$$h_m = \frac{h_c}{Lec_{p,a}} \tag{27}$$

The condenser is modeled in a similar manner with the evaporator from the modeling point of view. The mass, energy and momentum equations of the cell for refrigerant and pipe wall are the same as those for the evaporator. However, in the case of condenser, the superheated vapor, the two-phase and subcooled liquid regions are considered, whereas the evaporator is divided into the two-phase and superheat vapor regions. The initial and boundary conditions are different. A correlation developed by Shah is used to calculate the heat transfer coefficient during film condensation for annular flow [30]. At airside, the air humidity ratio doesn't change when it flows through the condenser. Therefore, only heat transfer occurs.

### 3.4. Expansion valve

The expansion valve can be modeled by the isenthalpic orifice. The mass flow rate through it can be correlated according to the following equation:

$$\dot{m}_{txv} = C_v A_{txv} \sqrt{\rho_{i,tvx} \Delta p_{txv}} \tag{28}$$

where $C_v$ is the flow coefficient. It depends on the degree of the valve openings. $A_{tvx}$ is the so-called "venacontracta " area. It could be considered as a minimum flow area across the orifice. In general, $A_{tvx}$ does not coincide with the orifice across sectional area. In equation, $\Delta p_{txv}$ is the pressure difference between the inlet and outlet of the expansion valve, and $\rho_{i,txv}$ is the refrigerant inlet density of expansion valve.

### 3.5. Performance indices

To evaluate the performance of the present system, air dehumidification rate (ADR), cooling power (Q) and COP are defined. ADR and Q reflect the overall effect of the total heat exchanger and the DX system. ADR and Q are calculated by the following equations:

$$ADR = ADR_{mem} + ADR_{DX} = V_a\rho_a(\omega_A - \omega_B) + V_a\rho_a(\omega_B - \omega_C) \tag{29}$$

$$Q = Q_{mem} + Q_{DX} = V_a\rho_a(H_A - H_B) + V_a\rho_a(H_B - H_C) \tag{30}$$

where $\omega$ is humidity ratio of membrane-based total heat exchanger; $\rho_a$ is density of air; $H$ is air enthalpy. Subscript A, B and C is air state points in Fig. 1.

For the present system, the total power consumption by the system is a sum of the fan and compressor power consumptions. $COP_{nov}$ is defined by

$$COP_{nov} = \frac{Q}{W_{fan} + W_{elec}} = \frac{Q}{W_{nov}} \tag{31}$$

where $W_{fan}$ is the fan power consumption. It can be calculated by:

$$W_{fan} = \frac{V_a \Delta p}{3600\eta_{fan}} \tag{32}$$

where $\Delta p$ is total pressure drop, $\eta_{fan}$ is fan efficiency.

The conventional DX dehumidification system is a vapor compression system. The $COP_{conv}$ is calculated by

$$COP_{conv} = \frac{V_a\rho_a(H_{ai} - H_{ao})}{W_{elec}} \tag{33}$$

where $W_{elec}$ is compressor power consumptions. $H_{ai}$ and $H_{ao}$ are the inlet and outlet enthalpy of evaporator of conventional air dehumidification system, respectively.

### 3.6. Numerical procedure of system model

The solution of the system model can be facilitated by taking advantage of the logical flow of information between the different

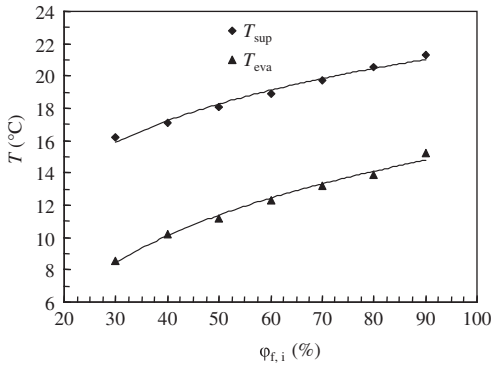


**Fig. 10.** Variations of evaporator temperature and supply air temperature with different inlet air relative humidity.

components. It proceeds from the evaluation of one component to the other, starting at the membrane-based total heat exchanger and proceeding down to the compressor, condenser, thermal expansion valve and evaporator, as shown in Fig. 5. When a component name is mentioned in the flow chart, the corresponding equations for each one are used. For example, when the "membrane-based total heat exchanger" is mentioned in the chart, the corresponding equations of (3) to (7) are used. The whole model constitutes a series of non-linear algebraic equations. The component models can be combined into a system model and appropriate outputs from each component model are provided as logical inputs to the other component models. Consequently, the solution to the system of equations can be reduced to two equations with respect to evaporator temperature and condenser temperature. The values of condenser temperature and evaporator temperature are found by using bisection method in the trial and error procedure. The fundamental parameters of the solution procedures like input and output are listed in the Table 2.

## 4. Results and discussions

### 4.1. Model validation

The ADRs and the COP are tested in the real system. The tested data are used to validate the present model. Figs. 6 and 7 are the comparisons between the experimental results and the calculated results. As seen, the predictions are acceptable. The deviations of predicted ADRs are within 10%, and the deviations of COP are within 5%. After the model validation, numerical work is performed in the following.

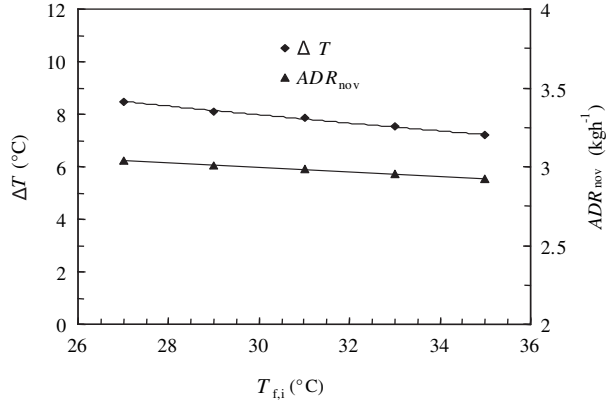


**Fig. 11.** Variations of air dehumidification rates and temperature difference between supply air and indoor air with different inlet air temperature.

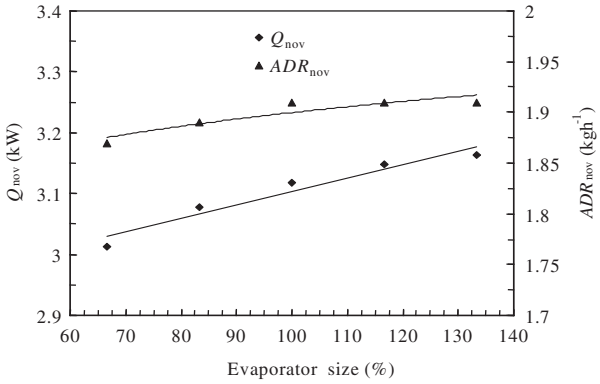


**Fig. 12.** Effect of the evaporator size on ADR and Q.

### 4.2. Effects of inlet air humidity

In subtropical regions like Guangzhou, the air relative humidity is very high, even 80–90% sometimes. Its effects should be considered. The variations of air dehumidification rates and supply to indoor air temperature differences are plotted in Fig. 8. The inlet air relative humidity changes, while other parameters are fixed at: $T_{f,i} = 35$ °C, $T_{ex,i} = 27$ °C, $\varphi_{ex,i} = 53\%$ and $V = 200$ m$^3$ h$^{-1}$. It is demonstrated that the ADR increases substantially with an increase in inlet air humidity. The ADR increases from 2.2 kg h$^{-1}$ to 4.5 kg h$^{-1}$ when the inlet air humidity increases from 50% to 90% RH.

The variations of $\varepsilon_L$ and SHR (sensible heat ratio, sensible to total load ratio at evaporator) with varying inlet air relative humidity are plotted in Fig. 9. As seen, the higher the air relative humidity is, the higher the $\varepsilon_L$ is. With a higher latent effectiveness, the moisture removed by the total heat exchanger increases. At the same time, the moisture removed by the evaporator also increases in humid conditions. The cooling power of the evaporator increases accordingly. However, the sensible cooling load at the evaporator decreases slightly due to the increased evaporator temperature at high humidity. As a result, the SHR decreases with an increase in inlet air humidity. This result agrees with the investigation conducted by Liang et al. [31]. In a summary, the ADR increases significantly with an increase in inlet air relative humidity.

From Fig. 8, it is also observed that the supply to indoor air temperature differences decrease with higher inlet air humidity. The temperature differences decrease from 8.9 °C to 5.7 °C with an increase in inlet air relative humidity from 50% to 90%. Though all these temperature differences are acceptable, they should be as small as possible from thermal comfort considerations [32]. An increased supply air temperature is beneficial for preventing cold

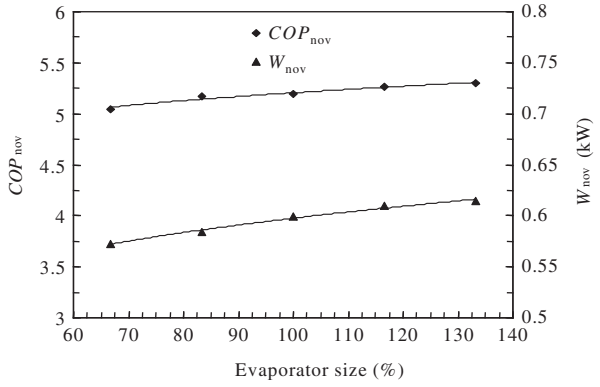


**Fig. 13.** Effect of the evaporator size on the COP and power consumptions.

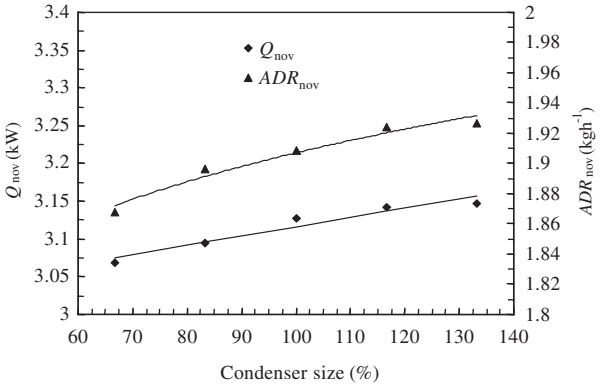


**Fig. 14.** Effect of the condenser size on ADR and *Q*.

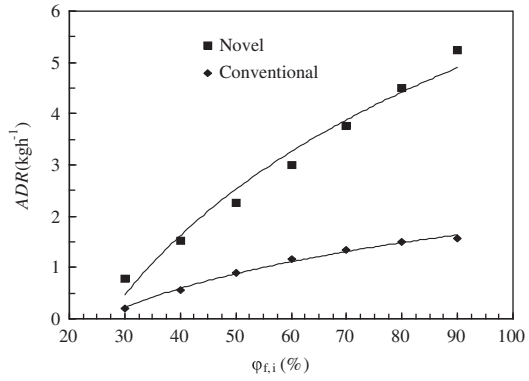


**Fig. 16.** Variations of air dehumidification rates for the two systems with different inlet air relative humidity.

draft. The variations of evaporator and supply air temperatures with inlet air relative humidity are potted in Fig. 10. As seen, the higher the inlet air relative humidity is, the higher the evaporator and supply air temperatures are. Under humid conditions, the refrigerant mass flow rate is increased to meet the demand of the increasing cooling power. The increased evaporator temperature leads to an increase in supply air temperature.

### 4.3. Effects of inlet air temperature

Effects of outside air temperature are interesting. The variations of air dehumidification rate and supply to indoor air temperature differences with various inlet air temperatures are plotted in Fig. 11. The fixed parameters are: $\omega_{f,i} = 0.021$ (kg moisture/kg air), $T_{ex,i} = 27$ °C, $\varphi_{ex,i} = 53\%$ and $V = 200$ m$^3$ h$^{-1}$. As seen, the ADR decreases slightly with an increase in inlet air temperature. Further, as the inlet air temperature increases, the temperature differences decrease whereas the latent effectiveness of the total heat exchanger is almost constant. Moisture removed by the total heat exchanger doesn't change. However, a higher inlet air temperature would increase the fin surface temperature a little bit. The driving force for mass transfer between air and fin surface decreases somewhat accordingly. Moisture removed by the evaporator decreases a little bit. Since most of the moisture is removed by the total heat exchanger, the total ADR decreases only slightly with an increase in inlet air temperature. As thermal comfort is concerned, the supply to indoor air temperature difference decreases with a higher inlet air temperature. Supplying air with dew points does not cause cold draft problems under hot and humid weather conditions. Therefore comparing to Ref. [14], this system is still promising. The new system is simpler.

### 4.4. Effects of evaporator and condenser sizes

Evaporator and condenser sizes have great impacts on the performances of the whole system such as ADR and *Q*. Their effects on the performances of the system are studied. The evaporator and condenser sizes range from 70% to 130% of the original sizes. The effects of the evaporator size on ADR and *Q* are shown in Fig. 12. As seen, the ADR increases significantly with increasing evaporator size from 70% to 100%. However, further increasing of the evaporator size from 100% to 130% will only have limited effects. The reason behind is that air dehumidification occurs mainly on the two-phase surfaces in the evaporator. The area of the two-phase surface increases with an increase in evaporator size below 100%. The area of the two-phase surface keeps invariant with an increase in evaporator size above 100%. In addition, Fig. 12 also shows that the *Q* and the cooling capability increase with the larger evaporator size. This is the result of the increased heat transfer area.

Fig. 13 shows the effects of the evaporator size on the COP and power consumptions. As seen, the COP and power consumptions show the increasing trend with the increasing evaporator size. The mass flow rate of refrigerant is increased to satisfy the increased *Q*. The power consumptions increase accordingly. However, the *Q* increase more than the power consumption does. Consequently, the COP increases with an increase in evaporator size.

The effects of the condenser size on ADR and *Q* are shown in Fig. 14. With an increase in condenser size, the heat transfer area increases and the condenser capacity increases accordingly. In this case, the condenser pressure decreases. As a result, the mass flow rate of refrigerant to the evaporator increases, which leads to evaporator capacity increasing. Finally, the ADR increases.

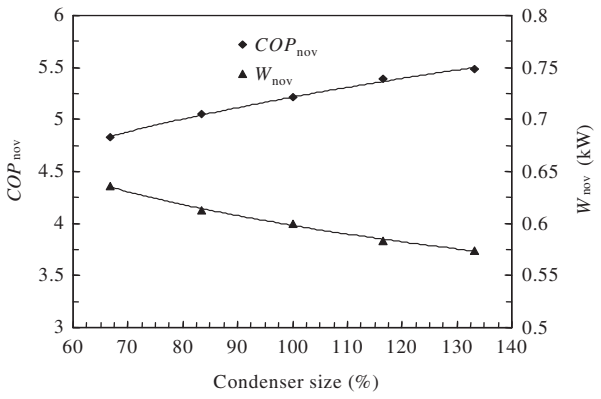


**Fig. 15.** Effect of the condenser size on the COP and power consumptions.

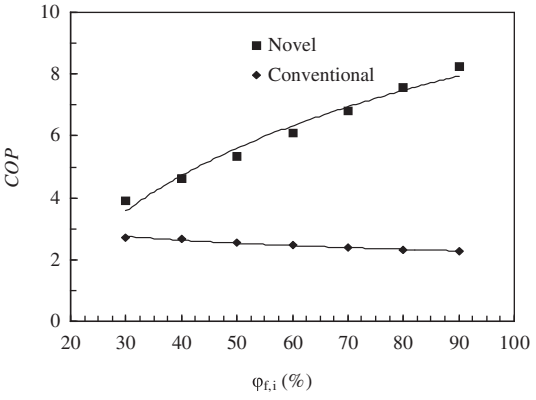


**Fig. 17.** Variations of COP for the two systems with different inlet air relative humidity.

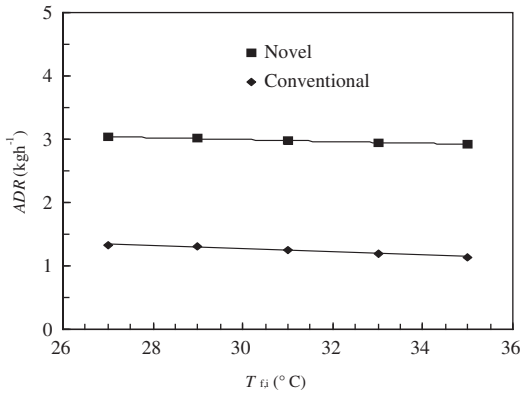


**Fig. 18.** Variations of air dehumidification rates for the two systems with different inlet air temperature.

Fig. 15 shows the effects of the condenser size on the COP and power consumptions. As seen, the larger the condenser is, the higher the COP is. This can be attributed to the fact that a larger condenser lowers the condensing pressure and thus decreases the compressor power consumptions. As a result, the COP increases and the power consumption decrease. Therefore, the above results demonstrate that the larger evaporator and condenser raise system performances.

### 4.5. Comparison with conventional DX dehumidification

Conventional DX systems are widely used in residential buildings and small-scale commercial buildings. However, the efficiency of DX dehumidification is insufficient in hot and humid environment. Figs. 16 and 17 show the variations of ADR and COP with inlet air relative humidity for the two systems (a DX air dehumidification system combined with membrane-based total heat recovery and a conventional DX dehumidification system). The fixed parameters are: $T_{f,i} = 35\ ^{\circ}C$, $T_{ex,i} = 27\ ^{\circ}C$, $\varphi_{ex,i} = 53\%$ and $V = 200\ m^3\ h^{-1}$. As can be seen, the novel system shows the higher ADR and COP than the conventional DX system. Furthermore, the ADR and the COP of the novel system increase at higher inlet air relative humidity. This is because the latent effectiveness of the total heat exchanger increases with an increase in the inlet air relative humidity. The results indicate that the DX air dehumidification system combined with membrane-based total heat recovery shows better efficiencies, especially in high humid environment.

Figs. 18 and 19 show the ADR and the COP for the two systems under different inlet air temperatures. The fixed parameters are: $\omega_{f,i} = 0.021$ (kg moisture/kg air), $T_{ex,i} = 27\ ^{\circ}C$, $\varphi_{ex,i} = 53\%$ and $V = 200\ m^3\ h^{-1}$. Fig. 18 shows that the ADR of the novel system is 1.5 times that of the conventional system. Fig. 19 shows that the COP of the novel system is 2 times that of the old system. Under higher inlet air temperatures, the ADR and the COP of the DX dehumidification system attenuate greatly whereas the new system attenuates slightly. The reason is that, most of the increased load is treated by the total heat exchanger, and only a small fraction is treated by the refrigeration system. The new system provides an alternative to available systems for air dehumidification [33–38].

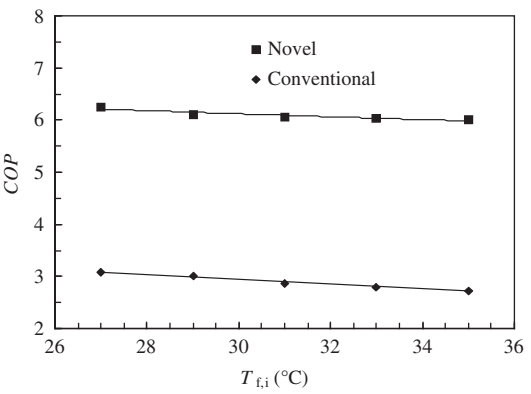


**Fig. 19.** Variations of COP for the two systems with different inlet air temperature.

## 5. Conclusions

A detailed simulation model based on cell-by-cell scheme is used to predict the DX system with membrane-based total heat exchanger recovery. The model is validated by the experimental data. The effects of inlet air humidity, temperature, evaporator, and condenser sizes on system performances are investigated. Following conclusions can be given:

(1) The model predicts the experiments well. The deviations of predicted ADRs are within 10%, and the deviations of COP are within 5%.
(2) Comparing with a conventional DX system, the present system has a high ADR and COP under hot and humid climates. This indicates the system has more robustness than the conventional refrigeration system under hot and humid harsh weather conditions. The higher the fresh air temperature and humidity are, the more effective the membrane-based total heat exchanger is. The membrane-based total heat exchanger improves the performances greatly. This compensates the performances of the compression subsystem which deteriorates seriously under hot and humid harsh conditions. The present system is a promising and efficient air dehumidification technology in hot and humid environment.
(3) The ADR of the novel system is 1.5 times that of the conventional system. The COP of the novel system is 2 times that of the old system.
(4) Supplying air with dew point does not cause cold draft problems under hot and humid weather conditions. The larger the inlet air temperature and humidity are, the less the temperature differences between supply air and the designed indoor air are. This has benefits for thermal comfort considerations.
(5) The effects of evaporator and condenser size on the performances of the system are studied. The evaporator and condenser sizes range from 70% to 130% of the original sizes. The ADR and COP improve with larger evaporators and condensers.

## Acknowledgements

This project is supported by the National High Technology Research and Development Program of China (863), 2008AA05Z206, Natural Science Foundation of China (No. 50676034), and the Fundamental Research Funds for the Central Universities, 2009ZZ0060.

## References

[1] Zhang YP, Yang R, Zhao RY. A model for analyzing the performance of photocatalytic air cleaner in removing volatile organic compounds. Atmospheric Environment 2003;37(24):3395–9.
[2] Mo JH, Zhang YP, Yang R. Novel insight into VOC removal performance of photocatalytic oxidation reactors. Indoor Air 2005;15(4):291–300.
[3] Xu Y, Zhang YP. An improved mass transfer based model for analyzing VOC emissions from building materials. Atmospheric Environment 2003;37(18):2497–505.
[4] Xu Y, Zhang YP. A general model for analyzing VOC emission characteristics from building materials and its application. Atmospheric Environment 2004;38(1):113–9.

[5] Liu XH, Zhang Y, Qu KY, Jiang Y. Experimental study on mass transfer performances of cross flow dehumidifier using liquid desiccant. Energy Conversion and Management 2006;47(15–16):2682–92.
[6] Liu XH, Li Z, Jiang Y, Lin BR. Annual performance of liquid desiccant based independent humidity control HVAC system. Applied Thermal Engineering 2006;26(11–12):1198–207.
[7] Zhang LZ. Total heat recovery: heat and moisture recovery from ventilation air. New York: Nova Science Publishing Co.; 2008. pp. 14. [Chapter 1].
[8] LeRoy JT, Groll EA, Braun JE. Computer model predictions of dehumidification performance of unitary air conditioners and heat pumps under extreme operating conditions. ASHRAE Transactions 1998;104(2):773–88.
[9] Turaga M, Lin S, Fazio PP. Performance of direct expansion plate finned tube coils for air cooling and dehumidification. International Journal of Refrigeration 1988;11(2):78–86.
[10] Xia L, Chan MY, Deng SM, Xu XG. Dehumidification effects in the superheated region (SPR) of a direct expansion (DX) air cooling coil. Energy Conversion and Management 2009;50(12):3063–70.
[11] Zhang LZ. Energy performance of independent air dehumidification systems with energy recovery measures. Energy 2006;31(8–9):1228–42.
[12] Zhang LZ, Zhu DS, Deng XH, Hua B. Thermodynamic modeling of a novel air dehumidification system. Energy and Buildings 2005;37(3):279–86.
[13] Zhang LZ. Air dehumidification. Beijing: China Chemical Industry Press; 2005.
[14] Liang CH, Zhang LZ, Pei LX. Independent air dehumidification with membrane-based total heat recovery: modeling and experimental validation. International Journal of Refrigeration 2009;33(2):398–408.
[15] Zhang LZ, Xiao F. Simultaneous heat and moisture transfer through a composite supported liquid membrane. International Journal of Heat and Mass Transfer 2008;51(9–10):2179–89.
[16] Guttman I, Wilks SS, Stuart HJ. Introductory Engineering Statistics. New York: John Wiley and Sons; 1965.
[17] Duprez ME, Dumont E, Frére M. Modelling of reciprocating and scroll compressors. International Journal of Refrigeration 2007;30(5):873–86.
[18] Lemmon EW, McLinden MO, Huber ML. NIST reference fluid thermodynamic transport properties—Refprop, version 7.0. USA: NIST; 2002.
[19] Browne MW, Bansal PK. Steady-state model of centrifugal liquid chillers. International Journal of Refrigeration 1998;21(5):343–58.
[20] Fu L, Ding GL, Su ZJ, Zhao GQ. Steady-state simulation of screw liquid chillers. Applied Thermal Engineering 2002;22(15):1731–48.
[21] Jin GY, Cai WJ, Wang YW, Yao Y. A simple dynamic model of cooling coil unit. Energy Conversion and Management 2006;47(15–16):2659–72.
[22] Wang FQ, Maidment GG, Missenden JF, Tozer RM. A novel special distributed method for dynamic refrigeration system simulation. International Journal of Refrigeration 2007;30(5):887–903.
[23] Corberan JM, De Cordoba PF, Gonzalvez J, Alias F. Semi-explicit method for wall temperature linked equations (SEWTLE): a general finite volume technique for the calculation of complex heat exchangers. Numerical Heat Transfer Part B: Fundamentals 2001;40(1):37–59.
[24] Wallis GB. One-dimensional two-phase flow. McGraw-Hill, Inc.; 1969.
[25] Collier J, Thome JR. Convective boiling and condensation. Oxford Science Publications; 1996.
[26] Whalley PB. Two-phase flow and heat transfer. Oxford University Press; 1996.
[27] Kilmenko VV. A generalized correlation for two-phase forced flow heat transfer. International Journal of Heat and Mass Transfer 1988;31(3):541–52.
[28] Threlkeld JL. Thermal environmental engineering. Prentice-Hall, Inc.; 1972.
[29] Wang CC. Performance of plate finned tube heat exchangers under dehumidifying conditions. Journal of Heat Transfer Engineering 1997;119(1):109–17.
[30] Shah MM. A general correlation for heat transfer during film condensation inside pipes. International Journal of Heat and Mass Transfer 1979;22(4):547–56.
[31] Liang SY, Liu M, Wong TN, Nathan GK. Analytical study of evaporator coil in humid environment. Applied Thermal Engineering 1999;19(11):1129–45.
[32] WHO-EHE 90. Indoor environment: health aspects of air quality, thermal environment, light and noise. Geneva: WHO; 1990.
[33] Worek WM, Moon CJ. Simulation of an integrated hybrid desiccant vapor-compression cooling system. Energy 1986;11(10):1005–21.
[34] Zubair SM. Improvement of refrigeration/air-conditioning performance with mechanical sub-cooling. Energy 1990;15(5):427–33.
[35] Fethi H, Imdat T, Mehmet G. The effect of the number of tube rows on heat, mass and momentum transfer in flat-plate finned tube heat exchangers. Energy 2001;26(11):963–72.
[36] San JY, Jan CL. Second-law analysis of a wet cross-flow heat exchanger. Energy 2000;25(10):939–55.
[37] Zubair SM. Thermodynamics of a vapor-compression refrigeration cycle with mechanical subcooling. Energy 1994;19(6):707–15.
[38] Tashtoush B, Molhim M, Al-Rousan M. Dynamic model of an HVAC system for control analysis. Energy 2005;30(10):1729–45.